

# Interpolation of surface radiative temperature measured from polar orbiting satellites to a diurnal cycle

## 1. Without clouds

Menglin Jin and Robert E. Dickinson

Department of Atmospheric Sciences, University of Arizona, Tucson

**Abstract.** The land surface skin temperature diurnal cycle (LSTD) is an important element of the climate system. This variable, however, cannot be directly obtained globally from polar orbiting satellites because such satellites only pass a given area twice per day and because their infrared channels cannot observe the surface when the sky is cloudy. To obtain the skin temperature diurnal cycle and fully utilize satellite measurements, we have designed an efficient algorithm that combines model results with satellite and surface-based observations and interpolates satellite twice-daily observations into the diurnal cycle. Climatological information from a climate model, CCM3/BATS, is used to determine a normalized shape (typical pattern) of the diurnal temperature for different latitudes, seasons, and vegetation types. The satellite observations, which are by themselves inadequate, are combined with the normalized modeled diurnal typical patterns to obtain the skin temperature diurnal cycle. The normalized typical patterns depend on the parameters of the diurnal insolation, such as sunrise, sunset, and peak times, and are also affected by the type of vegetation cover and soil moisture. The underlying physical foundation of this algorithm is that the diurnal cycle of temperature can be viewed as a composite of a daily average, diurnal periodic component, and random aperiodic component (noise). With the assumption that the noise can be ignored, the daily average can be inferred from satellite twice-per-day measurements and the periodic part can be obtained from modeled climatologies, providing a reasonable approach for estimation of the diurnal cycle of skin temperature. The general framework of the algorithm and its application for the clear-sky (cloud free) conditions are presented. This cloud-free version of algorithm is evaluated using FIFE and BOREAS field experiment surface observations. Regional tests over the Mississippi River basin have also been conducted using GOES-8 and AVHRR observations. Uncertainties of this cloud-free algorithm have been analyzed, indicating an accuracy of about 1–2 K for monthly cloud-free diurnal cycles at near-pixel resolution.

## 1. Introduction

Skin temperature refers to the effective radiative temperature of the Earth's surface. Sensible and latent fluxes of energy are proportional to the difference between this temperature and that of the overlying air. Over land, this difference and hence the energy fluxes are maintained by net radiative forcing minus changes in heat storage of the surface. Thus fluxes of sensible and latent heat together, typically more than  $500 \text{ W m}^{-2}$  for a nearly overhead Sun, are directly driven by this temperature difference which is from several up to  $10^\circ$  or more. The magnitude of the difference depends not only on net radiation minus the latent heat but also on wind and surface roughness, as determined by the type of vegetation cover, and on details of the atmospheric boundary layer [Crosson *et al.*, 1993; Betts and Ball, 1995; Garratt, 1995; Webster *et al.*, 1996]. The strongest control under clear-sky conditions, the diurnal cycle of net surface radiation, is relatively easy to determine and will vary primarily with latitude and season. What fraction of the solar radiation incident at the surface is absorbed is determined by the albedo, depending largely on the

type of vegetation cover and on the direction of the incident flux [Schluessel *et al.*, 1994; Sellers *et al.*, 1995]. Clouds affect surface temperature by reflection of solar radiation and by emission of downward longwave radiation, depending on cloud base, composition (water or ice), amount, and time of occurrence [Houze, 1993].

Skin temperature can be measured by radiometers, either at the surface for local sites or by instruments on aircraft or on satellites for larger areas. Satellite platforms provide global coverage, but effective use of their measurements requires a number of difficulties to be addressed. These include limitations of the satellite sampling and obstruction of the surface by clouds. Geostationary satellites provide diurnal coverage but are limited by a large field of view and limited coverage. Minnis and Harrison [1984] designed formulas from GOES half-hour interval measurements for daytime and nighttime and used them to calculate skin temperature for the time when the sky was covered by clouds. Their method did not address the dependencies on surface characteristics, soil moisture, or variations in surface insolation, but it did establish the possibility that a realistic skin temperature diurnal cycle might be obtained from satellite data.

Polar orbiting satellites in low orbit can provide much better spatial resolution and hence potentially more useful estimates of surface skin temperature than can other measurement

Copyright 1999 by the American Geophysical Union.

Paper number 1998JD200005.  
0148-0227/99/1998JD200005\$09.00

methods. Currently, such a measurement is provided by the split-window thermal channels on the advanced very high resolution radiometers (AVHRR) of the NOAA operational meteorological satellite series. It provides daily coverage of the Earth in four or five spectral bands at a resolution of 1 km, allowing estimation of surface temperature, vegetation coverage, surface albedo, and cloud detection [Price, 1984; Stowe *et al.*, 1991; Tucker *et al.*, 1991; Goward *et al.*, 1993]. Improved measurements will become available with the launch of the Moderate Resolution Imaging Spectroradiometer (MODIS) on the Earth Observing System (EOS) platforms AM in 1998 and PM in 1999, but these observations will continue to suffer the limitations of all polar orbiting satellites; that is, the surface can be observed at most twice a day and only under cloud-free conditions. Hence for measured skin temperatures to be used for various climatological studies such as flux computation and model evaluation, additional information as to the diurnal cycle of skin temperature and its modification in the presence of clouds must be developed.

The importance of the land surface temperature diurnal cycle (LSTD) and the need to obtain land skin temperature (LST) observations motivate this study. It develops a procedure for use of twice-per-day samples of skin temperature from a polar orbiting satellite to provide the diurnal skin temperature. Such a procedure must recognize the factors that significantly influence land surface temperature. Among these, the surface insolation is perhaps most important. It varies with latitude and season. Other surface characteristics, clouds, soil moisture, the boundary layer, and overlying atmosphere also impact on surface temperature and its diurnal change [Betts and Ball, 1995; Jin *et al.*, 1997; Ignatov and Gutman, 1998]. Vegetation cover affects surface temperature through its albedo [Charney *et al.*, 1977], as well as through its roughness and stomatal resistance [Henderson-Sellers, 1993]. Soil moisture has a significant influence on the surface skin temperature [Newton *et al.*, 1982; Hall *et al.*, 1995]. The difference between skin and air temperatures also depends on atmospheric wind and humidity. The many atmospheric and surface processes that influence surface temperature and its remote sensing are all interconnected. However, they need to be treated separately to reduce complexity for the design of an algorithm for data inversion.

Our algorithm combines satellite observations with model simulations. Generalization of the algorithm to the cloudy case would require in situ surface-based observations. The clear-sky algorithm has been tested using AVHRR and GOES measurements and is easily generalized to future polar orbiting imagers such as MODIS.

This paper outlines the general framework of the algorithm and its application to clear-day (cloud free) situations, as required before a treatment for the presence of the clouds can be developed. Section 2 introduces the data used in this work. Section 3 discusses the methodology. Section 4 gives the results and evaluation of the algorithm for cloud-free conditions. The uncertainties and limitations of this proposed algorithm are analyzed in section 5, and summary and conclusions are presented in section 6.

## 2. Data

Three kinds of data are used: satellite observations, surface-based field experiments, and CCM3/BATS hourly simulations. We derive the typical patterns of skin temperature diurnal

cycle from the model simulations and evaluate them using field experiments. Satellite observations and field experiments are also employed for algorithm validation.

### 2.1. Satellite Skin Temperatures

Measurements from NOAA-11 AVHRR instruments have been used for algorithm development and evaluation. AVHRR has two thermal infrared channels (ch4 and ch5) to observe surface temperature. One year (1993) of ch4 and ch5 daytime brightness temperatures have been obtained from the NOAA Goddard Space Flight Center Pathfinder Land Data Set [James and Kalluri, 1994]. Corresponding nighttime observations are available from a university archive [Rosborough *et al.*, 1994]. LST was calculated from ch4 and ch5 brightness temperatures by using a split-window algorithm that assumes a constant surface emissivity [Prata *et al.*, 1995] and corrects for water vapor effects. Besides LST, cloud masks for the daytime observations were obtained from the NOAA Pathfinder Land Data Set to determine the presence of clouds.

The geostationary satellite GOES observes the surface continuously at a nadir pixel resolution of about 4 km [Menzel and Purdom, 1994]. Its high temporal resolution allows an evaluation of our algorithm. Half-hourly GOES-8 IR brightness temperature were derived for 35°–40°N, 90°–100°W and July 1996, in the Mississippi River basin area, from original images of NOAA satellites [Menzel and Purdom, 1994] as used by Hsu *et al.* [1997].

### 2.2. Surface Measurements

Site-averaged surface observations were obtained for the First International Satellite Land Surface Climatology Project (ISLSCP) Field Experiment (FIFE), which was conducted over a 15 km × 15 km area in central Kansas from May 1987 to 1989 [Sellers *et al.*, 1992]. The site-averaged automatic meteorological station (AMS) data are processed by Betts and Ball [1995] for 1987, 1988, and 1989, starting from the summer of 1987 (May 26 to October 16). The AMS are 10 portable automatic meteorological (PAM) stations in the 15 × 15 km domain. This work uses the 1988 observations.

Surface observations are also obtained from the BOREAS (Boreal Ecosystem-Atmosphere Study) southern study area (SSA) near Prince Albert, Saskatchewan, for the 1996 experiment period [Sellers *et al.*, 1995, 1997].

### 2.3. Model Simulations

Hourly results from 1 year of a CCM3/BATS [Dickinson *et al.*, 1993; Kiehl *et al.*, 1996] simulation are used to estimate the monthly mean diurnal cycles. Ideally, the LSTD method designed here can be derived with observations. Since observational data are of limited coverage, this method is currently derived with model data for skin temperature. To the extent that observational data are free of errors or that the model represents reality, observations and model simulations should be essentially the same. The BATS model used here has an extensive history of use and is estimated to be as robust and reliable as any land model used as part of a climate model. Furthermore, its calculation of skin temperature has been evaluated against observations by Jin *et al.* [1997].

The primary requirement for the data used for estimation of the diurnal shape functions is that they span a wide range of the relevant parameter space, which includes all latitudes, seasons, and land covers. Available observations are much too limited for that purpose, so it is by necessity that model data

must be used. However, our confidence in the accuracies of the results inferred from the model simulations is improved by its validation against a limited number of local observational data sets [Hahmann *et al.*, 1995; Ward, 1995; Yang and Dickinson, 1996; Hahmann and Dickinson, 1997; Jin *et al.*, 1997].

### 3. Methodology

As Trenberth [1984] assumed for annual temperature, the diurnal cycle of temperature can be viewed as a composite of a diurnal average, daily periodic component, and random aperiodic component (noise). Thus

$$T_{\text{skin}}(t) = \bar{T}_{\text{skin}} + \Delta T_{\text{skin}}(t) + T'_{\text{skin}}(t), \quad (1)$$

where  $\bar{T}_{\text{skin}}$  is the daily average,  $\Delta T_{\text{skin}}(t)$  is the diurnal cycle which is presumably determined by the atmospheric-surface physical processes, and  $T'_{\text{skin}}(t)$  is the instantaneous disturbance from the mean conditions. This disturbance can be largely explained as the response of the atmospheric surface layer to short timescale atmospheric forcing, for example, by radiative effects of clouds or soil moisture changes by precipitation. The short timescale white noise of the atmospheric forcing has been argued to produce a red noise response [Delworth and Manabe, 1988]. Following the analysis of Delworth and Manabe, the disturbance  $T'_{\text{skin}}(t)$  can be considered the diurnal component of the red noise caused by the short-term atmospheric forcing and may have a persistence of up to weeks or more, as is determined by soil heat and water storage.

The basic assumption of our method is that the periodic component may vary in amplitude in response to past history and current meteorological conditions but that it has a shape which is invariant or varies at most with a limited number of known factors that do not change rapidly from day to day. These may include latitude or season because of their control of incident solar radiation, type of vegetation cover because of its effect on albedo and roughness, and soil moisture because of its effect on evapotranspiration. With this assumption of invariance, the daily periodic shape can be estimated from the averaging of a sufficient number of days of hourly data. Given this shape and assuming that any red noise component that does not follow this shape can be neglected, skin temperature has only two degrees of freedom, so twice a day measurements as from polar orbiting satellites (e.g. AVHRR or MODIS) can be used to estimate both the diurnal average and the daily periodic temperature components. In reality, it is unlikely that the random component in (1) will be negligibly small; however, this component of skin temperature may have substantial memory, as argued above. Hence the use of instantaneous measurements to fit the diurnal shape may also capture some of the random aperiodic component as well.

Figure 1 illustrates observational testing of (1) relating statistically skin temperature at 0400 or 1600 LT to that at other hours. Data are from FIFE July 1988 site-averaged hourly observations. Figure 1a shows a high correlation between 0400 LT temperature and other temperatures during the same night but a much smaller correlation with the subsequent daytime temperatures. Likewise, it also shows that the 1600 LT measurement correlates better with daytime values than with the subsequent nighttime values. Figure 1b, showing a measure of the root-mean-square difference of 0400 and 1600 LT temperatures to other temperatures, implies the same conclusions. The weak correlation between day and night temperatures may

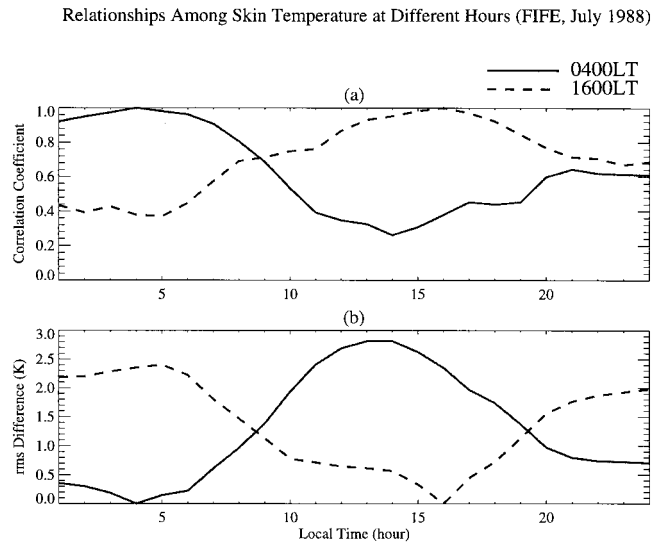


**Figure 1.** Temporal correlation (a) and root-mean-square difference (b) of  $T_{\text{skin}}$  at 0400 and 1600 LT with  $T_{\text{skin}}$  at other hours. The root-mean-square difference ( $d_4(j)$  and  $d_{16}(j)$ ) is defined as  $d_4(j) = \sqrt{(1/N) \sum_{i=1}^N (T_{i4} - T_{ij})^2}$ ,  $d_{16}(j) = \sqrt{(1/N) \sum_{i=1}^N (T_{i16} - T_{ij})^2}$ , where  $N$  is the number of days, from 1 to 31;  $j$  is hour, from 1 to 24;  $T_{i4}$  is skin temperature at 0400 LT, and  $T_{i16}$  is skin temperature at 1600 LT.

be a result of different physical processes determining temperatures. Evidently, at least one daytime and one nighttime value of temperature are necessary for estimating a realistic diurnal cycle, and so at least twice-per-day polar orbiting satellite measurements may be required to derive the temperature diurnal cycle.

Our method assumes that the shape of the skin temperature diurnal cycle can be adequately approximated with monthly mean observations. With this assumption, clear-day monthly mean diurnal cycles derived from CCM3/BATS hourly simulations are used as the typical shape of the diurnal cycle, referred to as “typical pattern” herein. These typical patterns are functions of vegetation type, season, and latitudes. We have evaluated how well the typical patterns match available field experiments and geostationary satellite observations. This evaluation concludes that the modeled typical patterns agree adequately with the observed monthly patterns, but as a monthly average, they cannot provide the correct temperature range of any single day because the day-to-day variations of the diurnal amplitudes are largely determined by each day’s instantaneous atmospheric and soil conditions. This suggests a need to use each day’s instantaneous measurements, for example, satellite twice-per-day data, to further adjust these typical patterns.

The general scheme of how an LSTD algorithm works is presented in Figure 2. In general, three predetermined data sets would be used: (1) typical patterns derived from model simulations as a function of latitude, season, vegetation type, and cloud amount; (2) surface air temperature, along with wind speed, humidity, and cloud conditions as routinely observed at surface weather stations to provide additional information for each day; and (3) relationships between skin and surface air temperatures as predetermined from atmospheric boundary layer theory and from model simulations.

The initial step is to read in satellite daily skin temperatures

## Scheme of LSTD Algorithm

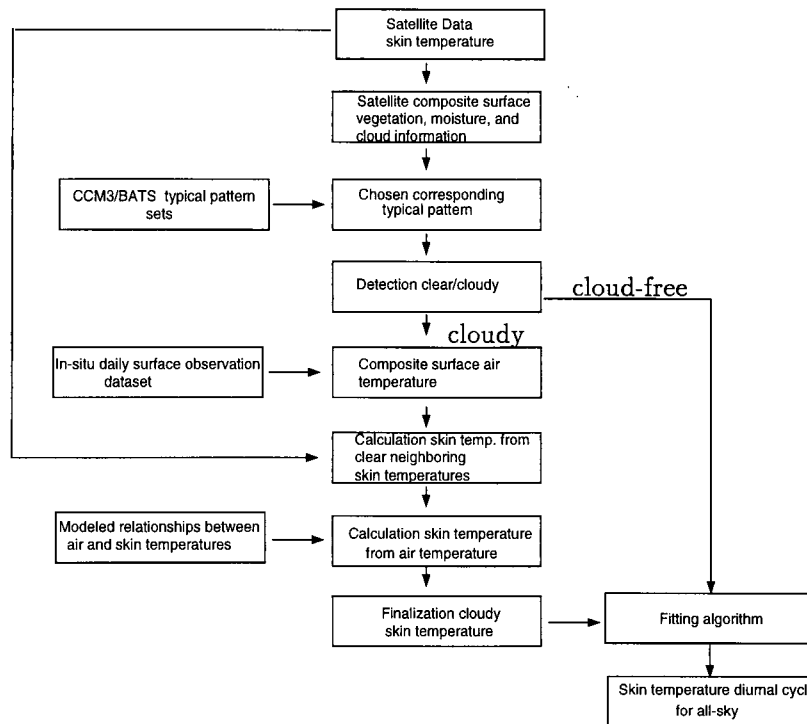


**Figure 2.** Flow diagram showing the major steps of the land surface diurnal cycle algorithm. See text for details.

for each location. Then further information for that time and place is needed, in particular, soil/vegetation type, soil moisture, and the state of the overlying atmospheric column, such as cloud cover. Vegetation coverage, vegetation type, and surface greenness change slowly such that we can use 10 day or biweekly information. A corresponding typical pattern for the location is then selected on the basis of cloud, moisture, vegetation, latitude, and season conditions and is used to match the skin temperature measurements by use of a fitting routine. This paper describes the clear-sky fitting process for LSTD.

To generalize from the treatment in this paper to cloudy conditions where satellite measurements of skin temperature would not be directly available requires determining skin temperature from measured values at the neighboring clear pixels and using local air temperature as a constraint. Then, similar to the cloud-free case, the estimated skin temperature can be used to fit the corresponding model-derived typical pattern.

## 4. Results

### 4.1. Typical Patterns

This paper uses the vegetation categories defined for BATS [Dickinson *et al.*, 1993, Table 1]. Figure 3 shows the July typical pattern of skin temperature diurnal cycle for crop/mixed farming over 40°–45°N. We sampled and analyzed all model grids within this latitude band for this vegetation cover, average soil moisture, and clear days. Figure 3a shows a box-and-whiskers diagram representing the range of data. The box in the middle of the diagram is bounded by the upper and lower quartiles and thus locates the central 50% of the data. The bar inside the box locates the median [Wilks, 1995]. The whiskers extend

away from the box to extreme values showing the range from 2.5% to 97.5% of the data. Figure 3b gives the diurnal cycle with the daily average subtracted to remove much of the latitudinal influence of surface insolation and to facilitate comparison.

The diurnal pattern of temperature depends not only on the

CCM3/BATS Monthly Mean Diurnal Cycle, Veg1, July (40–45°N)

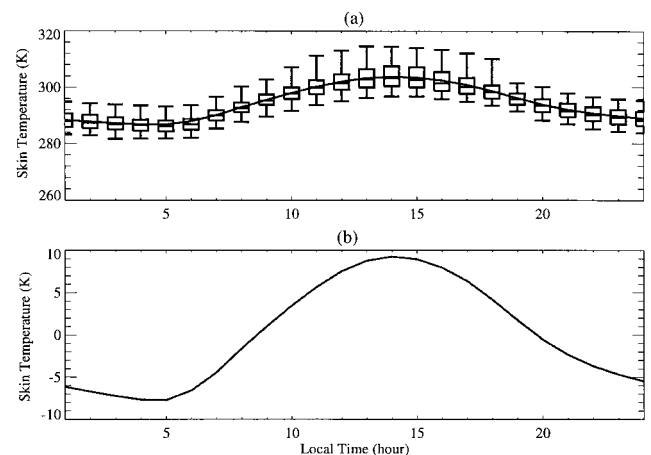


**Figure 3.** Grid-averaged monthly mean skin temperature diurnal cycle for July, clear sky. Data are from model hourly simulations; all grids vegetated by crop/mixed farming over 40°–45°N are sampled. (a) Diurnal cycle. (b) Diurnal cycle with the daily average removed from each sample.

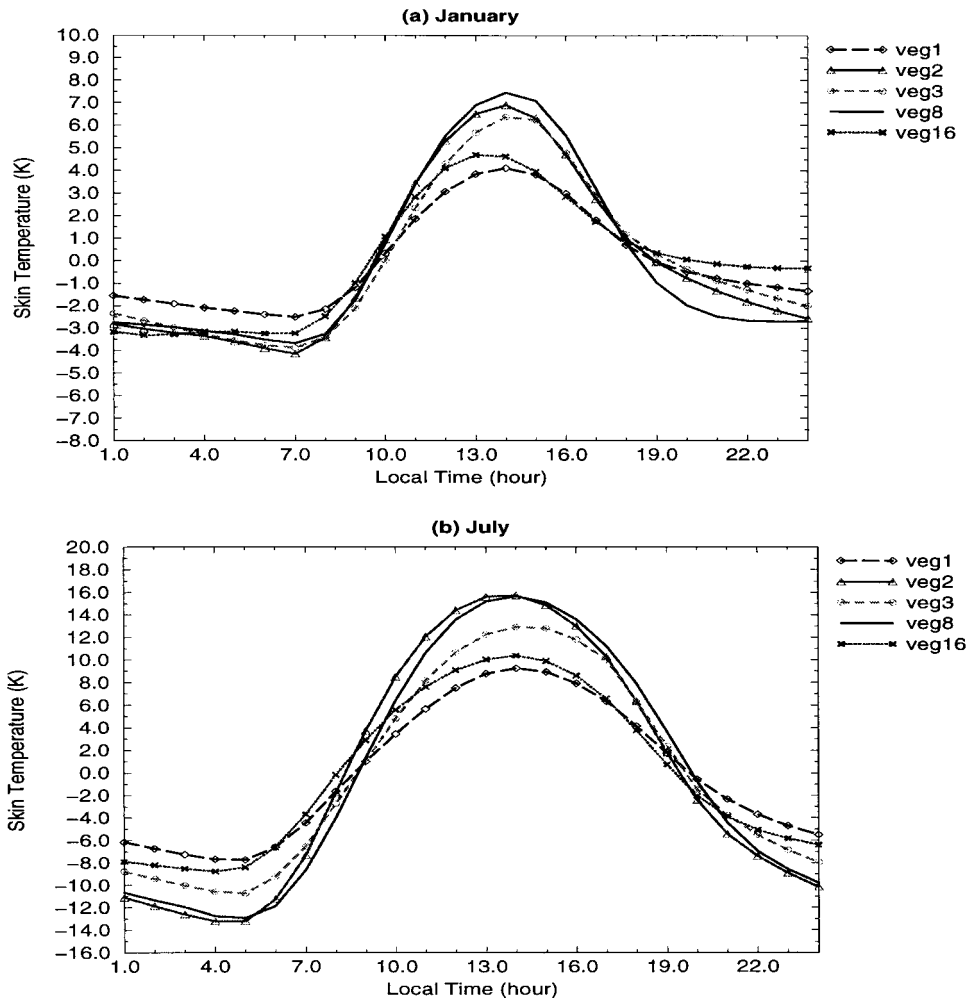


**Figure 4.** Modeled monthly diurnal cycles of skin temperature over  $40^{\circ}$ – $45^{\circ}$ N for different vegetation types. The mean has been removed for each curve. (a) January, (b) July. Data are analyzed from hourly CCM3/BATS simulations. Veg1: crop/mixed farming; veg2: short grass; veg3: evergreen needleleaf tree; veg8: desert; and veg16: evergreen shrub.

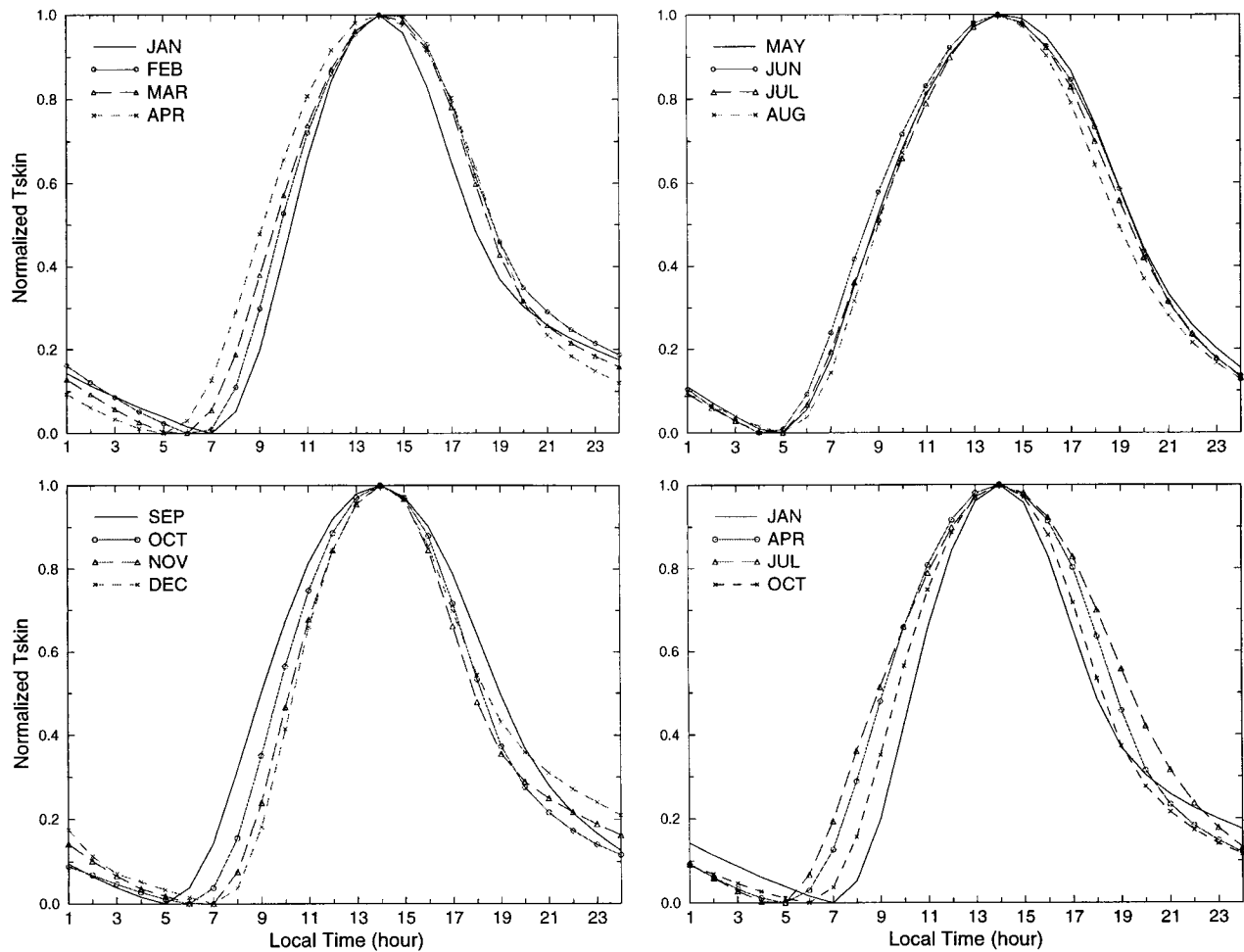
daily range but also on the slope and phase of the heating and cooling. In order to make all these parameters obvious, a simple normalization procedure is used. For each monthly mean diurnal cycle (as in Figure 3b), the formula  $\hat{T}(i) = (T(i) - T_{\min}) / (T_{\max} - T_{\min})$  is used, where  $i$  is the hour from 1 to 24. These normalized patterns are the “typical patterns” used herein. They can be compared to each other regardless of season or latitude. As later shown, this method captures the most significant features of a diurnal cycle and reduces the number of typical patterns required to produce a global data set.

Figure 4 shows the dependence of the monthly LST diurnal cycle on vegetation type for clear-sky monthly values at  $40^{\circ}$ – $45^{\circ}$ N. Evidently, different vegetation types have quite different ranges, phases, peak times, and daily means. Besides vegetation cover, solar insolation, and soil moisture also determine the diurnal range. The normalization of typical patterns reduces this dependence, but some residual effects remain, as illustrated by Figures 5–7. Figure 5, for crop/mixed farming vegetation at  $40^{\circ}$ – $45^{\circ}$ N, illustrates how seasonally changing diurnal patterns of solar radiation influence the diurnal temperature patterns. The most noticeable controls are the times

of peak, sunset, and sunrise. Figure 6, for the crop/mixed farming and for July, shows that the patterns are also dependent on latitude, largely because of different day lengths.

Figure 7 examines the normalized clear-case typical patterns of LSTD for different moisture conditions, over  $40^{\circ}$ – $45^{\circ}$ N. The wet case is defined as an average over surfaces with a Bowen ratio less than 0.3 and the dry case for a Bowen ratio larger than 1.5. Generally, greater amplitudes result from drier surfaces [Bastable and Shuttleworth, 1993]. However, the normalized typical patterns, with the amplitude of diurnal range removed, are fairly similar. The dry pattern lags the normal and the wet patterns because a larger fraction of solar radiation goes into heating the soil. This result is consistent with FIFE observations [Betts and Ball, 1995, Figure 1]. Although the nonnormalized dry surface temperatures and their rate of increase in the morning exceed those of the wet surface at all times (Figure 7b), the normalization along with its 1 hour phase lag acts in the morning (Figure 7a) to make the curve for the dry surface to fall below that of the wet one. Evidently, soil moisture information could be included in determining the typical pattern by delaying the peak time for dry conditions and advancing it for wet. However, in the absence of such moisture

## Typical Patterns in Different Months



**Figure 5.** Variations of typical patterns with month and season for the same vegetation type, crop/mixed farming, over clear-sky  $40^{\circ}$ – $45^{\circ}$ N. Data are monthly averages from hourly CCM3/BATS simulations. Abscissa is local time, and ordinate is normalized skin temperature (dimensionless).

data the normal-case typical pattern may give an adequate determination of LSTD since effects of moisture on the diurnal range of skin temperatures are already included through the observations.

The model-derived typical patterns have been evaluated by comparing them with the site-averaged observations for 1988 FIFE (Figure 8). The FIFE area is mostly covered by short grass. Thus we use typical patterns for short grass in this evaluation. The monthly skin temperature diurnal cycles from FIFE agree with the modeled typical pattern quite well, with rms (root-mean-square) less than 0.5 K for each season. The diurnal patterns are also validated against data for the BOREAS forest area at  $50^{\circ}$ – $55^{\circ}$ N (Figure 9). Some differences are seen, especially for the forest. Our research suggests that these differences are amplified by the normalization procedure (not shown). They may reflect soil moisture effects, differences between assumed and actual vegetation, random effects, or defects in the model climate simulations. In addition, the model typical pattern is derived from all grids with the same

### Solar Radiation Effects

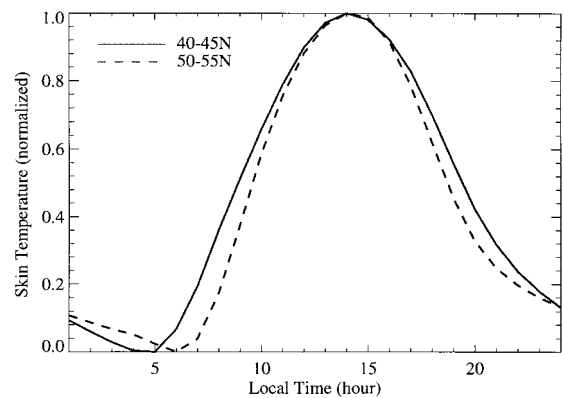


**Figure 6.** Comparison between the modeled typical patterns at different latitudes for vegetation type 1, crop/mixed farming. The typical patterns are for July, clear sky.

vegetation type within the latitude band, but the observations are only over one site or several sites, and the local conditions may be different from the large-scale averages. The correspondence between modeled and observed typical patterns in Figures 8 and 9 suggests that the model typical pattern adequately represents the shape of the diurnal cycle. However, some measured values are needed to pin down its average value and range.

Statistical analyses indicate that 0400 and 1600 LT (when the AVHRR passes through a given longitude at local time) temperature differences have a significant correlation with the diurnal range. Table 2 shows that the daily range of temperature can be calculated from 0400 and 1600 LT values for all vegetation types and have correlation coefficients higher than 0.90. Hence it appears that the daily range can be inferred to some degree from satellite observations at these two times.

The examples in Figures 5–7 show a dependence of the diurnal temperature pattern on sunset, sunrise, and peak time. The timing of minimum temperature, in general, is closely related to the sunrise time [Sellers, 1965] and the timing of maximum skin temperature to solar insolation peak time, with some phase lag. From the peak time until sunset and from sunset to midnight, the temperature decreases following different functions. A simple formula can represent the typical pattern as a function of sunset, sunrise, peak times, and other constants associated with the analytic shape of the four curves, as suggested in Figure 10. Consequently, the typical patterns

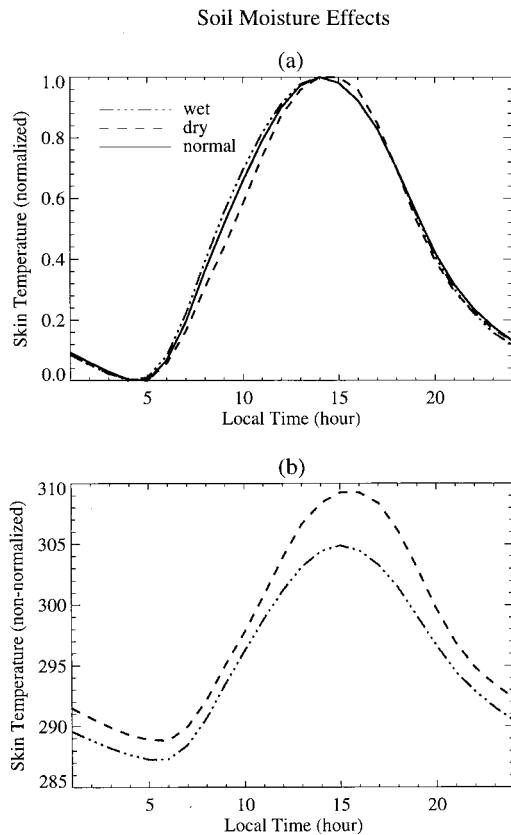


**Figure 7.** (a) Comparison between the modeled typical patterns at different soil moisture conditions for vegetation type 1, crop/mixed farming. The typical patterns are for July, clear sky. (b) Same as Figure 7a except for the nonnormalized diurnal patterns.

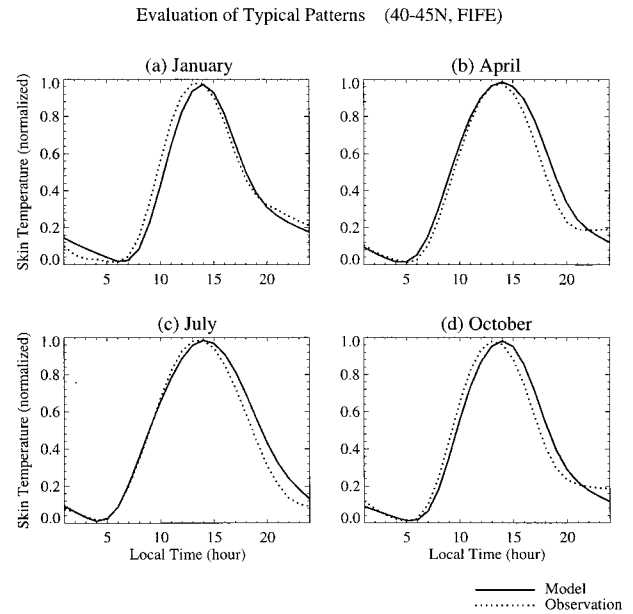


**Figure 8.** Comparison between the typical patterns and normalized FIFE monthly observations. FIFE observations are site averaged, and the typical patterns are derived from hourly CCM3/BATS simulations. For each month, only clear days are analyzed. (a) January, (b) April, (c) July, and (d) October.

for all latitudes, seasons, vegetation types, and soil conditions can be described in a look-up table.

**4.2. Cloud-Free Algorithm**

As defined in Figure 2, the “cloud-free algorithm” includes reading in satellite-measured twice-per-day skin temperature, information about surface vegetation, moisture, and cloud conditions; retrieving the predefined CCM3/BATS typical pattern

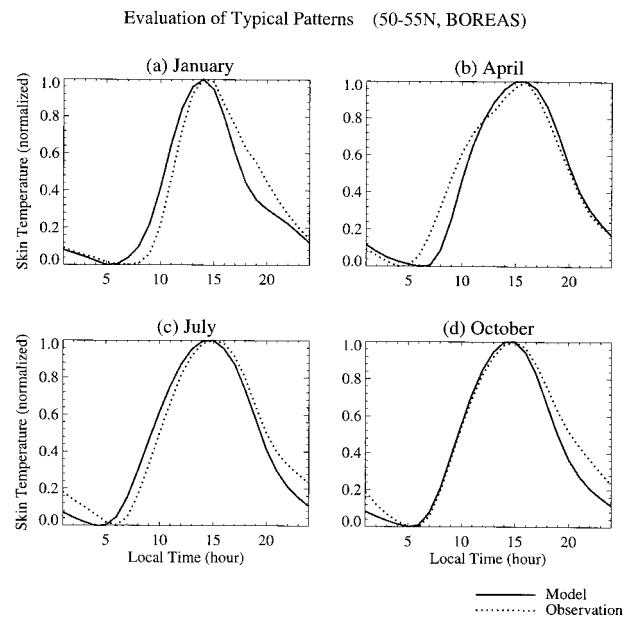


**Figure 9.** Same as Figure 8 except for BOREAS. Vegetation type over BOREAS is evergreen needleleaf tree. (a) January, (b) July, (c) August, and (d) September.

**Table 1.** Vegetation/Land Cover Types

Vegetation Type	Name	Vegetation Type	Name
1	crop/mixed farming	9	tundra
2	short grass	10	irrigated crop
3	evergreen needleleaf tree	11	semidesert
4	deciduous needleleaf tree	12	ice cap/glacier
5	deciduous broadleaf tree	13	bog or marsh
6	evergreen broadleaf tree	16	evergreen shrub
7	tall grass	17	deciduous shrub
8	desert	18	mixed woodland

Copied from BATS [Dickinson *et al.*, 1993]

for the read-in surface and atmospheric conditions; then determining if the pixel is cloud free. For the clear pixels, the fitting algorithm is called to combine the satellite temperatures with the retrieved typical pattern to interpolate the diurnal cycles.

This cloud-free algorithm applies when the sky is effectively clear during the whole day, and the two satellite measurements are available to adjust the typical pattern. Figure 11 shows the cloud-free algorithm-produced diurnal cycle for the clear days in 1988 over FIFE. Figures 11a, 11b, and 11c are January, July, and September, representing winter, summer, and fall, respectively. FIFE 0400 and 1600 LT measurements are used to fit the typical pattern. In these months, clear days are determined by comparing the solar insolation with the solar radiation at the top of the atmosphere for each daylight hour. If the former is more than 80% of the latter during the whole daytime, it is regarded as a clear day. Cloud conditions at night are not used to determine clear days. The mean values of algorithm-produced and observed diurnal cycles agree to root-mean-square errors of around 2 K. Over the FIFE area the algorithm is more accurate in summer than it is in winter (rms is 1.86 K in July while 2.27 K in January). Larger cloud contamination occurs at night and in winter for the year and place examined. The rms value at night was 3.04 K for January but 2.35 K for July. Whether or not the reduced accuracy during winter 1988 applies climatologically would require analysis of a much longer time series of data.

Clear days from BOREAS (July 1996) have also been used to test our algorithm. Figure 12a is the same as Figure 11

**Table 2.** Correlation Coefficient ( $T_{1600LT} - T_{0400LT}$ ) and Diurnal Range ( $T_{max} - T_{min}$ ) for Each Vegetation Type at 40°–45°N

Vegetation Type	January	April	July	October
1	0.98	0.967	0.990	0.989
2	0.959	0.966	0.988	0.982
3	0.994	0.971	0.977	0.989
5	0.981	0.981	0.999	0.989
7	0.987	0.954	0.999	0.992
8	0.969	0.986	0.985	0.994
10	0.971	0.924	1.000	0.989
11	0.944	0.988	0.981	0.993
16	0.943	0.902	0.984	0.979
18	0.984	0.978	0.894	0.993

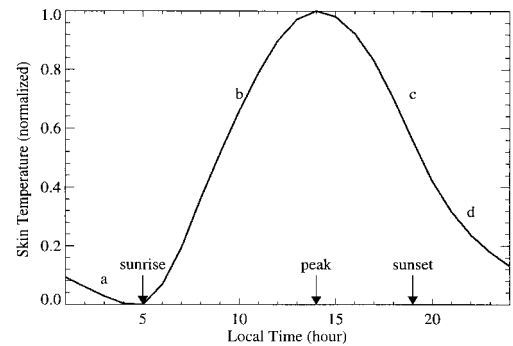
Vegetation type is defined in BATS (1, crop/mixed farming; 2, short grass; 3, evergreen needleleaf tree; 5, deciduous needleleaf; 7, tall grass; 8, desert; 10, irrigated crop; 11, semidesert; 16, evergreen shrub; 18, mixed woodland). Data are from hourly model simulations.

except for BOREAS. There were nine clear days in this period. Figure 12b is the average of these nine days. Differences between observations and the algorithm in Figures 11 and 12 may result when the sky is significantly covered by clouds at hours other than those used for the solar insolation test for clear skies, or at night when a clear-sky test is not applied. Therefore the daily temperature variations cannot be more precisely estimated without referring to more frequent observations and without more elaborate modeling that recognizes the period of cloud cover. The rms error of the algorithm is about 1 K for the BOREAS case and 2 K for FIFE.

Sometimes satellite observations can be missing or only give a daytime value. A modified version of our algorithm can treat this situation. However, with only a daytime value, the estimate of LST diurnal cycle is much less accurate. Figure 13 is a test using only the daytime skin temperature to adjust the typical pattern. The increase in error is quite obvious (rms is 2.61 K compared to 1.86 K for use of two values) and greatest at night, as expected from Figure 1. Thus if fewer than two observations are available in a 24 hour period, additional information, as described for the cloudy case, is needed.

**4.2.1. GOES-8 Evaluation.** We obtained GOES-8 measurements at half-hour intervals over the area (35°–45°N, 90°–100°W), in the Mississippi basin, for the purpose of further evaluating our algorithm. This area is dominated by mixed farming and tall grass (corresponding to BATS vegetation types 1 and 7).

IR brightness temperatures and temporal and spatial threshold methods [Minnis and Harrison, 1984; Rossow *et al.*, 1985; Coakley, 1987] are used to detect cloud pixels. First, spatial histograms are analyzed to tentatively identify clear pixels by the values in the warm end of the histogram. Then, each clear



$$\begin{aligned}
 (1) : T_{skin}(t) &= A - Bt \\
 (2) : T_{skin}(t) &= \sin(\pi(t - t_{sunrise} - 1)/length - a_1\phi) \\
 (3) : T_{skin}(t) &= \sin(\pi(t - t_{sunrise} - 1)/length - a_2\phi) \\
 (4) : T_{skin}(t) &= (t_{sunset} - 2) - ((t - t_{sunset} - 1)/2)^b \\
 \text{note : } \phi &= (t_{sunset} - t_{sunrise} - 12) * \pi / (12)^2 \\
 \text{or : } \phi &= (t_{peak} - 12) * \pi / (12)^2 \\
 \text{length} &= t_{sunset} - t_{sunrise}
 \end{aligned}$$

**Figure 10.** Simplification of the typical pattern. The arrows show the sunrise, sunset, and peak, when the temperature reaches its maximum. These times vary with season and vegetation type. Curve a is from 0100 LT to sunrise and curve b from sunrise to the peak time; curve c is from peak time to sunset and curve d from sunset to midnight. A simple expression is given as an example to describe the above curve, where  $t$  is local time, ranging from 1 to 24, and  $T_{skin}(t)$  is the normalized temperature at time  $t$ ;  $a_1$  and  $a_2$  are constants varying with seasons and vegetation types.

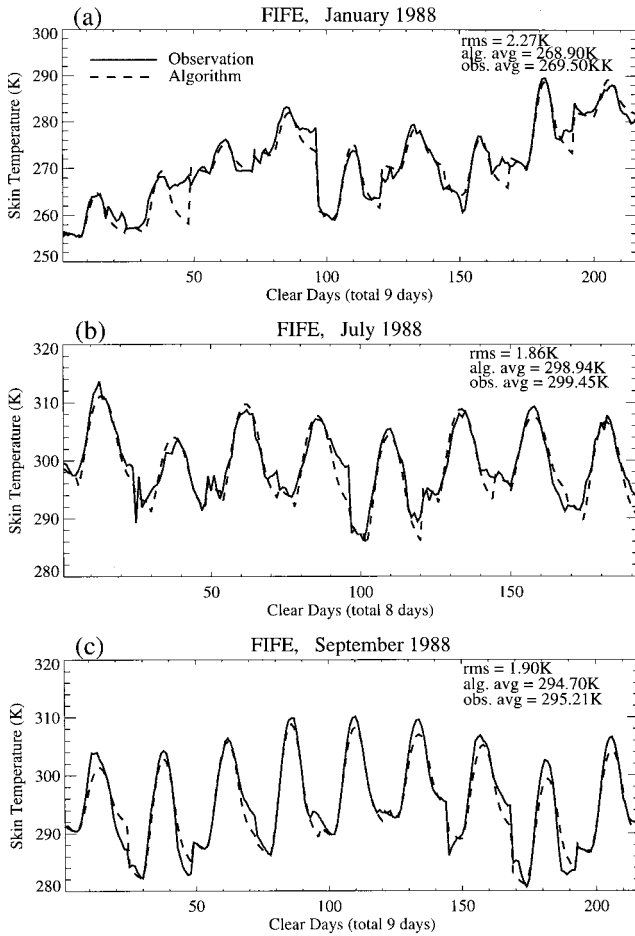


**Figure 11.** Comparison of the algorithm-produced diurnal cycles with FIFE observations. (a) January, (b) July, and (c) September. Only clear days in each month are analyzed. The clear days are determined using the daytime solar insolation. See text for detail.

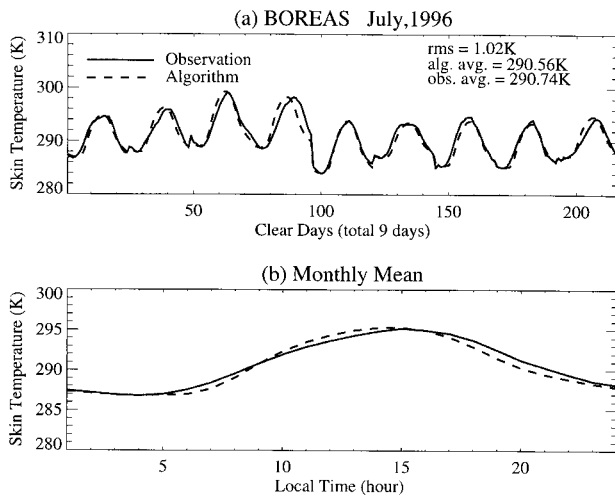


**Figure 12.** (a) Same as Figure 11 except over BOREAS forest, July 1996. There were nine clear days in this month. (b) Monthly mean of the algorithm-modeled diurnal cycles and the observations for the clear days are presented in Figure 12a.

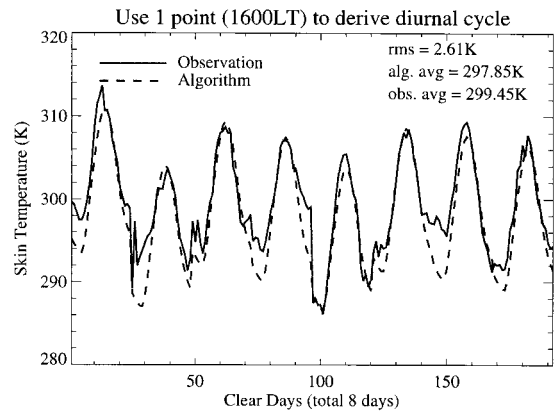


**Figure 13.** Comparison of the algorithm-modeled diurnal cycle with FIFE observations. The algorithm-produced diurnal cycle was retrieved using one time (1600 LT) of FIFE observation.

pixel is compared with the highest value of that pixel over a 15 day period. A difference smaller than 6 K is flagged as clear, otherwise the pixel is detected as cloudy. This method likely rejects some clear situations as cloudy. However, by doing so, it establishes clear situations with relatively high confidence.

Figure 14 is the histogram of skin temperatures for the selected area on July 2, 1996. This day is chosen because, as

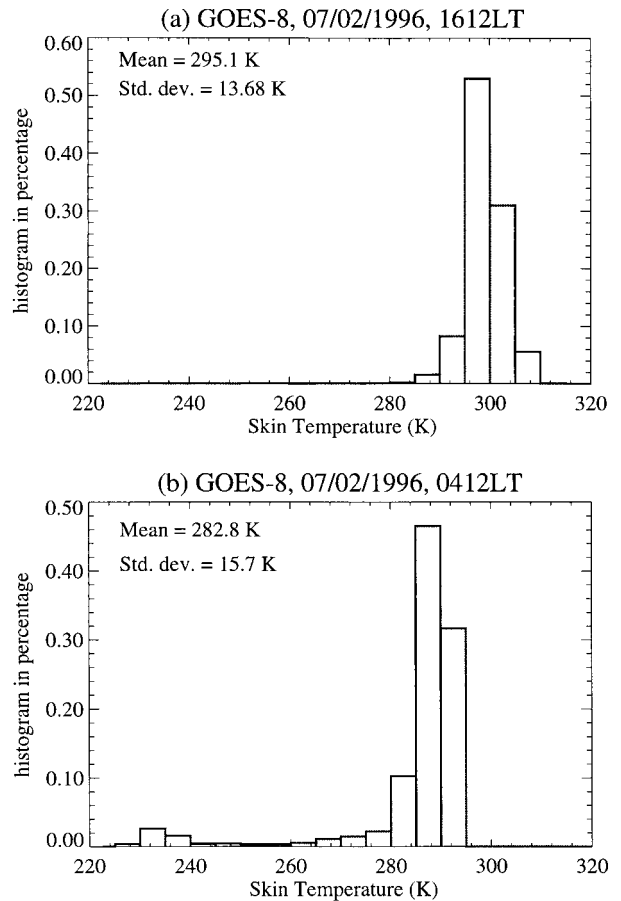


**Figure 14.** Histograms of GOES observations on July 2, 1996, over 35°–45°N, 100°–90°W. (a) Daytime observations at 1612 LT and (b) nighttime observations at 0412 LT.

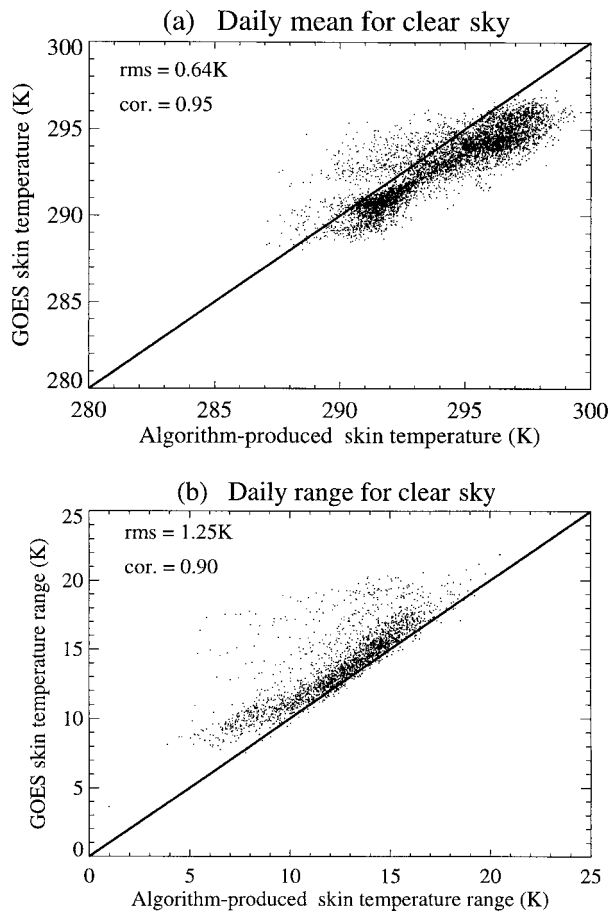


**Figure 15.** Comparisons between algorithm-produced diurnal cycles and GOES observations: (a) daily mean and (b) daily range for one day (July 2, 1996). GOES-8 observations are over the area  $35^{\circ}$ – $45^{\circ}$ N,  $100^{\circ}$ – $90^{\circ}$ W. Only clear pixels are analyzed.

presented, most of the pixels are clear, as determined by the preceding described detection method. Pixels falling into the warm end at these two times are considered as clear pixels. Over this region, mean temperature for the daytime (1612 LT) is 295.1 K with a standard deviation of 13.68 K. At night (0412 LT) the region-averaged temperature decreases to 282.8 K with a standard deviation of 15.7 K. These twice-daily observations provide information as to the true skin temperature and are used to fit the CCM3/BATS-derived typical patterns to obtain the diurnal cycle.

To evaluate the algorithm that assumes only two measurements available a day, we estimate whether a GOES pixel is clear or cloudy from 1 day and one night measurement. Then LSTD is retrieved on the basis of the day and night measurements for this pixel estimated to be clear. This estimated LSTD is then compared with the GOES observations over the rest of the day to evaluate the accuracy of our algorithm and to understand what factors affect its accuracy. Clear pixels were determined from 1612 and 0412 LT measurements, corresponding to the overpass time of the NOAA-11 polar orbit. Using identified clear pixels and their 1600 and 0400 LT temperatures to fit the typical pattern, we can estimate the diurnal cycles. These estimates can then be tested with the GOES half-hourly observations to evaluate the algorithm.

Figure 15 compares the algorithm-produced daily mean and range with that of the GOES observations for each clear pixel on July 2, 1996. The algorithm-produced diurnal cycle agrees adequately with that of the observations, with an rms error about 0.64 K for daily mean and 1.25 K for daily range. The largest contribution to the rms error in the diurnal range is from extreme values of some pixels where the GOES-observed daily ranges are about 15 K larger than those produced by the algorithm. We found these pixels to be significantly contaminated by colder temperatures from clouds or precipitation that occurred between the twice-daily GOES observations (at 1612 and 0412 LT) which identified the sky conditions as clear. If these partially cloudy pixels are deleted, an accuracy of 0.5–1 K is found for the daily range. Hence the cloud-free algorithm appears to work adequately for a completely clear day. However, the presence of partial or short-period cloud cover may evidently degrade its accuracy.

**4.2.2. AVHRR Evaluation.** Further evaluations were also conducted for the same Mississippi basin area using 1 km AVHRR polar orbiting measurements for June 1993. The results (not shown) agree with those from GOES-8. For a given location the AVHRR data were measured approximately at 0200 and 1400 LT. The average and difference of these twice-per-day AVHRR temperatures are considered as the “true” daily mean and daily range. After using these two AVHRR-based skin temperatures to develop the diurnal cycle, the algorithm daily mean is the average of the 24 hourly values, and the daily range is the difference between maximum and minimum. For pixels completely clear for the whole day, our cloud-free algorithm can produce a very realistic diurnal cycle with the level of random errors no more than 1.5 K. If clouds occur at other times during the day than when skin temperatures are measured, the error of the algorithm estimates will be substantially increased.

## 5. Algorithm Uncertainty Analysis

Inaccuracy of the satellite data, uncertainties of the modeled typical pattern, and limitations of the fitting method designed for this algorithm are the largest sources of error. Remote sensing researchers, for example, *Wan* [1996] and *Becker and Li* [1995], state that the satellite LST data can achieve an accuracy of 1 K. They require making several assumptions about surface state, aerosol effects, and atmospheric properties before a radiative transfer model can retrieve skin temperature. The assumed surface emissivity used in LST retrieval potentially causes some error. Because LST and surface emissivity can only be obtained individually from a radiative transfer model by knowing the other, most LST algorithms assume that the surface emissivity is uniform, from 0.88 for HIRS-2 (R. Haskins, personal communication, 1998) to 0.98 for MODIS [*Wan*, 1996], leading to an error in LST of about 1 K. We estimate that CCM3/BATS gives the diurnal shape of the monthly average of skin temperature at 0.5–1 K accuracy for most areas, based on our data comparisons. Because errors in satellite data, model typical patterns, and fitting procedure are independent, the total accuracy of our algorithm can be estimated to be about 1.5–2 K over a monthly average for one pixel, consistent with our results presented earlier. The accuracy of the algorithm described here is not significantly lower than that of its input observations and should provide useful diurnal cycles at near-pixel resolutions. Use of differences,

rather than the absolute values of skin temperature, could remove the systematic errors existing in the absolute values.

Cloud contamination reduces the accuracy of the derived diurnal cycle of skin temperature. Either a "cloudy algorithm," as described in Figure 2, can be applied or the microwave-based measurements used. Microwave-based land surface skin temperature data sets may in the future achieve an accuracy of about 1 K at 1° resolution for the monthly mean values (A. Basist, personal communication, 1998). However, this is a much coarser spatial resolution than that of the imaging IR channels for which this algorithm is designed.

## 6. Summary

The global diurnal cycle of skin temperature is needed for many land surface studies. Only satellites can provide the needed measurements. However, it has not been previously possible to obtain adequate global descriptions of diurnal variations of skin temperature. Polar orbiting satellites observe land surface temperature only twice daily, whereas geostationary satellites observe a fixed area continuously but only cover part of the globe. Hence to obtain an adequate description of the diurnal cycle of surface temperature as required for land surface study, model and other observations must be used to supplement satellite measurements.

The retrieval of LST by polar orbiting satellites has high spatial resolution and global coverage. Such a LST, however, cannot be directly used by models to improve their surface processes and flux calculations because models require the details of a diurnal temperature cycle which are not provided directly by the satellite product. This work develops the use of twice-a-day temperature measurements of polar orbiting satellites to provide the needed diurnal information.

The algorithm assumes that the diurnal cycle is a composite of daily average, daily periodic component, and random aperiodic component (noise). The periodic component may vary in amplitude in response to past or current atmospheric and surface conditions, but its shape does not vary rapidly from day to day and thus can be obtained from modeled temperature climatologies. Ignoring the noise, we can infer the daily average from satellite daily observations and by combining satellite data and model results to reasonably derive the diurnal cycle of skin temperature.

Given the above, an efficient algorithm is developed to interpolate twice-per-day polar orbiting satellite measurements into the diurnal cycle for clear skies. The climate model CCM3/BATS is employed for such an interpolation. Each day's satellite observations are used to fit the typical patterns to obtain the diurnal cycle. The "cloud-free algorithm" is presented and analyzed in this paper. Field experiments, together with GOES and AVHRR satellite data, have been used to evaluate this algorithm. The accuracy of the "cloud-free" algorithm is about 1–2 K for monthly means at near-pixel resolution. Errors result from inaccuracies of the satellite data, model, or the algorithm itself. However, a combination of satellite, model, and surface observations constrain the fitted diurnal cycle of skin temperature to an acceptable accuracy.

The effects of solar radiation, vegetation type, and soil moisture are addressed in this clear-sky version of algorithm. Typical clear-sky patterns of a skin temperature diurnal cycle are determined from model simulations as a function of solar insolation, surface/vegetation type, and soil moisture. The most important parameters controlling the diurnal patterns are

the times of sunrise, sunset, and peak, which vary with latitude and season.

**Acknowledgments.** We thank the two anonymous reviewers for their constructive and insightful comments which helped us improve this manuscript. We also thank W. Emery's group at the University of Colorado for nighttime AVHRR data and S. Sorooshian's group at the University of Arizona for providing GOES data. This work is supported by the NASA graduate student fellowship and by the NASA EOS Interdisciplinary Scientific Research Program (U.P.N. 429-82-22; U.P.N. 428-81-22).

## References

- Bastable, H. G., and W. J. Shuttleworth, Observations of climate, albedo, and surface radiation over cleared and undisturbed Amazon forest, *Int. J. Climat.*, *13*, 13,783–13,796, 1993.
- Becker, F., and Z. Li, Surface temperature and emissivity at various scales: Definition, measurement and related problems, *Remote Sens. Rev.*, *12*, 225–253, 1995.
- Betts, Alan K. and J. H. Ball, The FIFE surface diurnal cycle climate, *J. Geophys. Res.*, *100*, 25,679–25,693, 1995.
- Charney, J. G., W. J. Quirk, S. H. Chow, and J. Kornfield, A comparative study of the effects of albedo change on drought in semi-arid regions, *J. Atmos. Sci.*, *34*, 1366–1385, 1977.
- Coakley, James A., A dynamic threshold method for obtaining cloud cover from satellite imagery data, *J. Geophys. Res.*, *92*, 3985–3990, 1987.
- Crosson, W. L., E. A. Smith, and H. J. Cooper, Estimation of surface heat and moisture fluxes over a prairie grassland, 4, Impact of satellite remote sensing of slow canopy variables on performance of a hybrid biosphere model, *J. Geophys. Res.*, *98*, 4979–4999, 1993.
- Delworth, T. L., and S. Manabe, The influence of potential evaporation on the variabilities of simulated soil wetness and climate, *J. Clim.*, *1*, 523–547, 1988.
- Dickinson, R. E., A. Henderson-Sellers, and P. J. Kennedy, Biosphere-Atmosphere Transfer Scheme (BATS) version 1E as coupled to the NCAR Community Climate Model, *NCAR Tech. Note, NCAR/TN-387+STR*, 72 pp., Natl. Cent. for Atmos. Res., Boulder, Colo., 1993.
- Garratt, J. R., Observed screen (air) and GCM surface/screen temperatures: Implications for outgoing longwave fluxes at the surface, *J. Clim.*, *8*, 1360–1368, 1995.
- Goward, S. N., D. G. Dye, S. Turner, and J. Yang, Objective assessment of the NOAA global vegetation index data product, *Int. J. Remote Sens.*, *14*, 3365–3394, 1993.
- Hahmann, A. N., D. M. Ward, and R. E. Dickinson, Land surface temperature and radiative fluxes response of the NCAR CCM2/biosphere-atmosphere transfer scheme to modifications in the optical properties of clouds, *J. Geophys. Res.*, *100*, 23,239–23,252, 1995.
- Hahmann, A. N., and R. E. Dickinson, RCM2-BATS model over tropical South America: Applications to tropical deforestation, *J. Clim.*, *10*, 1944–1964, 1997.
- Hall, F. G., J. R. Townshend, and E. T. Engman, Status of remote sensing algorithms for estimation of land surface state parameters, *Remote Sens. Environ.*, *51*, 138–156, 1995.
- Henderson-Sellers, A., A factorial assessment of the sensitivity of the BATS land-surface parameterization scheme, *J. Clim.*, *6*, 227–247, 1993.
- Houze, R. A., Jr., *Cloud Dynamics*, Academic, San Diego, Calif., 1993.
- Hsu, K., X. Gao, S. Sorooshian, and H. Gupta, Precipitation estimation from remotely sensed information using artificial neural networks, *J. Appl. Meteorol.*, *36*(9), 1176–1190, 1997.
- Ignatov, A. M., and G. G. Gutman, Land surface temperature diurnal cycle for global hydrological studies, *Adv. Space Res.*, in press, 1998.
- James, M. E., and S. N. V. Kalluri, The pathfinder AVHRR land data set: An improved coarse resolution data set for terrestrial monitoring, *Int. J. Remote Sens.*, *15*, 187–208, 1994.
- Jin, M., R. E. Dickinson, and A. M. Vogelmann, A Comparison of CCM2/BATS skin temperature and surface-air temperature with satellite and surface observations, *J. Clim.*, *10*, 1505–1524, 1997.
- Kiehl, J. T., J. J. Hack, G. B. Bonan, B. A. Boville, B. P. Briegleb, D. L. Williamson, P. J. Rasch, Description of the NCAR Community Climate Model (CCM3), *NCAR Tech. Note, NCAR/TN-420+STR*, 152 pp., Natl. Cent. for Atmos. Res., Boulder, Colo., 1996.
- Menzel, W. P., and J. F. W. Purdom, Introducing GOES-I: The first of

- a new generation of Geostationary Operational Environmental Satellites, *Bull. Am. Meteorol. Soc.*, *75*, 757–781, 1994.
- Minnis, P., and E. F. Harrison, Diurnal variability of regional cloud and clear-sky radiation parameters derived from GOES data, I, Analysis method, *J. Climatol. Appl. Meteorol.*, *23*, 993–1011, 1984.
- Netton, R. W., Q. R. Black, S. Mankanvand, A. J. Blanchard, and B. R. Jean, Soil moisture information and thermal microwave emission, *IEEE Trans. Geosci. Remote Sens.*, *21*, 300–307, 1982.
- Prata, A. J., V. Caselles, C. Coll, J. A. Sobrino, and C. Otle, Thermal remote sensing of land surface temperature from satellites: Current status and future prospects, *Remote Sens. Rev.*, *12*, 175–124, 1995.
- Price, J. C., Land surface temperature measurements from the split window channels of the NOAA 7 advanced very high resolution radiometer, *J. Geophys. Res.*, *89*, 7231–7237, 1984.
- Rossov, W. B., et al., ISCCP cloud algorithm intercomparison, *J. Climatol. Appl. Meteorol.*, *24*, 877–903, 1985.
- Rosborough, G. W., A. G. Baldwin, and W. J. Emery, Precise AVHRR image navigation, *IEEE Trans. Geosci. Remote Sens.*, *32*, 644–657, 1994.
- Schluessel, G., R. E. Dickinson, J. L. Privette, W. J. Emery, and R. Kokaly, Modeling the bidirectional reflectance distribution function of mixed finite plant canopies and soil, *J. Geophys. Res.*, *99*, 10,577–10,600, 1994.
- Sellers, P. J., F. G. Hall, G. Arsar, D. E. Strebel, and R. E. Murphy, An overview of the First International Satellite Land Surface Climatology Project (ISLSCP) Field Experiment (FIFE), *J. Geophys. Res.*, *97*, 18,345–18,371, 1992.
- Sellers, P. J., et al., The Boreal Ecosystem-Atmosphere Study (BOREAS): An overview and early results from the 1994 field year, *Bull. Am. Meteorol. Soc.*, *76*, 1549–1577, 1995.
- Sellers, P. J., et al., BOREAS in 1997: Experiment overview, scientific results, and future directions, *J. Geophys. Res.*, *102*, 28,731–28,769, 1997.
- Sellers, W. D., *Physical Climatology*, 272 pp., Univ. of Chicago Press, Chicago, Ill., 1965.
- Stowe, L. L., E. P. McClain, R. Carey, P. Pellegrino, G. G. Gutman, P. Davis, C. Long, and S. Hart, Global distribution of cloud cover derived from NOAA/AVHRR operational satellite data, *Adv. Space Res.*, *3*, 51–54, 1991.
- Tucker, C. J., W. W. Newcomb, S. O. Los, and S. D. Prince, Mean and inter-year variation of growing-season normalized difference vegetation index for the Sahel 1981–1989, *Int. J. Remote Sens.*, *28*, 46–45, 1991.
- Trenberth, K. E., Some effects of finite sample size and persistence on meteorological statistics, II, Potential predictability, *Mon. Weather Rev.*, *112*, 2369–2379, 1984.
- Wan, Z., MODIS land-surface temperature algorithm theoretical basis document (LST ATBD), NASA contract NAS5-31370, 1996.
- Ward, D. M., Comparison of the surface solar radiation budget derived from satellite data with that simulated by the NCAR CCM2, *J. Clim.*, *8*, 2824–2842, 1995.
- Webster, P. J., C. A. Clayson, and J. A. Curry, Clouds, radiation, and the diurnal cycle of sea surface temperature in the tropical western Pacific, *J. Clim.*, *9*, 1712–1730, 1996.
- Wilks, D. S., *Statistical methods in the atmospheric sciences*, An introduction, Academic, San Diego, Calif., 1995.
- Yang, Z.-L., and R. E. Dickinson, Description of the Biosphere-Atmosphere Transfer Scheme (BATS) for the soil moisture workshop and evaluation of its performance, *Global Planet. Change*, *13*, 117–134, 1996.

---

R. E. Dickinson and M. Jin, Department of Atmospheric Sciences, University of Arizona, Tucson, AZ 85721. (e-mail: menglin@air.atmo.arizona.edu)

(Received November 4, 1997; revised August 18, 1998; accepted August 25, 1998.)